Anomalous diffusion in a lattice-gas wind-tree model

X. P. Kong and E. G. D. Cohen
The Rockefeller University, 1230 York Avenue, New York, New York 10021
(Received 23 March 1989)

Two new strictly deterministic lattice-gas automata derived from Ehrenfest's wind-tree model are studied. While in one model normal diffusion occurs, the other model exhibits abnormal diffusion in that the distribution function of the displacements of the wind particle is non-Gaussian, but its second moment, the mean-square displacement, is proportional to the time, so that a diffusion coefficient can be defined. A connection with the percolation problem and a self-avoiding random walk for the case in which the lattice is completely covered with trees is discussed.

I. INTRODUCTION

Ehrenfest's wind-tree model[1] has contributed much to the understanding of kinetic processes in gases. Originally introduced to clarify the nature of the Stoszzahl ansatz in the Boltzmann equation, it was further studied about 20 years ago by Hauge and one of us[2] in connection with the divergences that occur in the density expansion of the transport coefficients in a moderately dense gas. The model consists of randomly placed diamonds (trees) in the plane, with parallel diagonals between which independent point (wind) particles can move, reflecting from the trees in one of four directions, that can be taken to be the $\pm x$ and $\pm y$ axes. The wind particles all have the same speed. The trees, although hard for the wind particles, can be "hard" for each other (nonoverlapping, NOV) or "soft" for each other (overlapping, OV). By using density expansions to compute the diffusion coefficient D of the wind particles through the trees, it was found that in the NOV case, the mean-square displacement $\Delta(t)$ of the wind particles was proportional to the time t, so that a diffusion coefficient could be defined and computed to second order in the tree density ρ. In the OV case, however, an abnormal diffusion process was discovered, due to excessive backscattering of wind particles by overlapping trees. In this case $\Delta(t)$ was not proportional to t—in fact, it increased slower than t—and no diffusion coefficient could be defined.[2] Furthermore, in analogy with the percolation problem it was surmised that, for the OV case, a critical tree density ρ_c existed below which the model exhibited—albeit abnormal—diffusive behavior, while above ρ_c no diffusion would occur, since all particles would be trapped, and $\Delta(t)$ would be bounded by a constant for large time t.[2,3] Later, Gates[4] introduced several lattice versions of the wind-tree model and rigorously proved for those models that for sufficiently high ρ, there is a complete absence of diffusion.

In all these cases the abnormal behavior implied that

$$\lim_{t\to\infty}\Delta(t)=\lim_{t\to\infty}\langle\Delta x^2\rangle=2Dt \tag{1}$$

was violated in that either $\Delta(t)$ grows slower in time or is bounded by a constant. Here Δx is the displacement of a wind particle in the x direction and the average is over a canonical ensemble of trees.

Recently, with the advent of cellular-automaton fluids,[5] lattice gases with particles moving through fixed scatterers have been considered.[6,7] The model mainly studied in this paper (model A) is a new deterministic lattice-gas wind-tree model.[8] This model is introduced in Sec. II, where the diffusion coefficient in the Boltzmann approximation is also derived. In Sec. III the simulation results for the diffusion coefficient and the deviations from the Boltzmann result are discussed. In Sec. IV the non-Gaussian distribution function and the kurtosis of the diffusion process are given. In Sec. V, the connection with the percolation problem and the possible evidence of a dynamical phase transition will be considered. In the last section, Sec. VI, results for a different lattice wind-tree model (model B) are presented.

II. THE MODEL AND THE BOLTZMANN DIFFUSION COEFFICIENT

The model considered here is a lattice wind-tree model. In this model scatterers (the trees) are randomly put at the sites of a square lattice with unit lattice constant, which then behave as two-sided mirrors. These mirrors, that can align along either one of the diagonal directions of the square lattice, will be called left or right mirrors, depending on the direction of alignment (Fig. 1). A wind particle (photon) with unit speed and four possible directions can propagate along the bonds of the lattice and be reflected by the scatterers. Two versions of the model have been considered: the mirrors are fixed (model A) or they flip to the other diagonal direction after being hit by the wind particle (model B). In this paper we will mostly be concerned with model A.

Starting from a particular lattice site at $t=0$, the positions of the wind particles are considered only at integer times, so that the system is a deterministic, time-reversal-invariant lattice-gas cellular automaton and the Boolean field description introduced by Frisch *et al.*[9] can be used for the motion of the wind particle. Thus, the basic equations of motion for the wind particles are

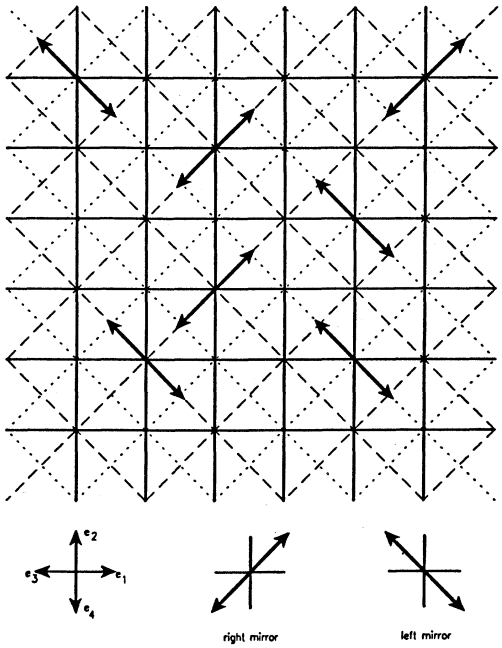

FIG. 1. Typical mirror configuration on the lattice. Dotted and dashed lines indicate the two sublattices, respectively, double arrows indicate the mirrors.

$$n_i(\mathbf{r}+\mathbf{e}_i,t+1)=(1-m_L-m_R)n_i+m_R n_{i+1}+m_L n_{i-1}\ , \quad (i=1,3)$$

$$n_i(\mathbf{r}+\mathbf{e}_i,t+1)=(1-m_L-m_R)n_i+m_R n_{i-1}+m_L n_{i+1}\ , \quad (i=2,4) \tag{2}$$

where $\mathbf{e}_i (i=1,2,3,4)$ is the unit velocity in the direction i (see Fig. 1). The n_i, m_L, and m_R are the Boolean fields of the wind particle with velocity $\mathbf{e}_i$, the left and the right mirrors, respectively. They all have the values 0 or 1 and on the right-hand side of Eq. (2) the dependence on $\mathbf{r}$ and t has been suppressed. Here $\mathbf{r}$ is the position of the wind particle at time t and the components of $\mathbf{r}$ as well as t take only integer values. In the Boltzmann approximation, the collisions of the wind particle with the scatterers (mirrors) are uncorrelated, and the Boltzmann equations for the one-particle distribution functions

$$f_i(\mathbf{r},t)=\langle n_i(\mathbf{r},t)\rangle\ ,$$

the ensemble average of the Boolean fields of the wind particle, reads

$$f_i(\mathbf{r}+\mathbf{e}_i,t+1)-f_i(\mathbf{r},t)=\sum_{j=1}^{4} T_{ij}f_j(\mathbf{r},t)\ , \quad (i=1,2,3,4)\ , \tag{3}$$

where the T_{ij} are the elements of the collision matrix:

$$T=\begin{bmatrix} -C_R-C_L & C_R & 0 & C_L \\ C_R & -C_R-C_L & C_L & 0 \\ 0 & C_L & -C_R-C_L & C_R \\ C_L & 0 & C_R & -C_R-C_L \end{bmatrix}, \tag{4}$$

with

$$C_L=\langle m_L\rangle, C_R=\langle m_R\rangle\ , \tag{5}$$

the concentrations of the left and right mirrors, respectively. When $C_L=C_R$, Eq. (3) is very similar to the Boltzmann equation for the continuous Ehrenfest wind-tree model.[10]

The diffusion coefficient D_B associated with the Boltzmann Eq. (3) can be derived straightforwardly, using the method of Ernst and Binder.[7] One finds

$$D_B=\phi_B-\tfrac{1}{4}\ , \tag{6}$$

where ϕ_B is the Boltzmann approximation to the usual velocity autocorrelation function formula of the diffusion coefficient

$$\phi=\sum_{t=0}^{\infty}\langle v_x(0)v_x(t)\rangle$$

so that[7]

$$\phi_B=\left\langle v_x\left|\frac{1}{1-\xi(1+T)}\right|v_x\right\rangle\Big|_{\xi=1}\ . \tag{7}$$

Here the (row) vector $\langle v_x|=(1/\sqrt{2})(1,0,-1,0)$, while its transpose, the (column) vector $|v_x\rangle$, is the x component of the velocity of the wind particle in the $\mathbf{e}_i$ basis. The $-\frac{1}{4}$ contribution to D_B is a contribution that appears in general in the Green-Kubo autocorrelation formulas for the transport coefficients due to the discreteness in space of the lattice gas (see the Appendix).

The eigenvalue problem associated with the matrix (4) is easily solved and yields the eigenvalues

$$\lambda_1=0,\quad \lambda_2=-2(C_L+C_R)=-2C\ ,\quad \lambda_3=-2C_L,\quad \lambda_4=-2C_R \tag{8}$$

with the corresponding orthonormal eigenvectors

$$|\lambda_1\rangle=\frac{1}{2}\begin{bmatrix}1\\1\\1\\1\end{bmatrix},\quad |\lambda_2\rangle=\frac{1}{2}\begin{bmatrix}1\\-1\\1\\-1\end{bmatrix},\quad |\lambda_3\rangle=\frac{1}{2}\begin{bmatrix}1\\1\\-1\\-1\end{bmatrix},\quad |\lambda_4\rangle=\frac{1}{2}\begin{bmatrix}1\\-1\\-1\\1\end{bmatrix}. \tag{9}$$

Inserting the projection operator

$$\sum_{i=1}^{4}|\lambda_i\rangle\langle\lambda_i|$$

into (7), one obtains

$$\phi_B = \frac{C}{8C_L C_R} \ . \tag{10}$$

For the case $C_L = C_R = C/2$, one has then

$$D_B = \frac{1}{2C} - \tfrac{1}{4} \ , \tag{11}$$

consistent with previous results.[8]

III. THE DIFFUSION COEFFICIENT FROM THE SIMULATIONS

The simulation results reported in this and the following sections were obtained for square lattices of typically 1024×1024 sites with several thousand wind particles on it. Unlike Ref. 8, where the wind particles always started at the lattice sites of a close-packed region in the center of the lattice and where consequently nearby particles had a good chance of following the same path, here the particles are put randomly through the lattice, which resulted in much better statistics. The simulation usually ran for several thousand time steps, occasionally extending to 100 000 time steps. In all simulations, periodic boundary conditions were used for the configurations of the scatterers. That is, while the wind particle moves in the infinite checkerboard, the trees are arranged periodically.

The time dependence of the diffusion coefficient D, as defined by Eq. (1), is for some mirror concentrations and $C_L = C_R = C/2$, given in Fig. 2. One sees that D indeed reaches a flat plateau, independent of t, after a rather long time, in agreement with Ref. 8. In fact, the number of time steps for this to occur can be in excess of 2000 for concentrations around $C = 0.8$. The dependence of D on the concentration C of the mirrors is given in Fig. 3 for fixed $t = 4000$, when D has reached its plateau value for all C. It is clear that D only agrees with D_B [Eq. (11)] for small C, as expected, but the deviations from D_B are small for all C. The deviations are positive, except for concentrations C close to 1, contrary to those caused by memory effects (long time tails), that are always negative.[2,3] The reason for these positive deviations of D from D_B are indeed due to an entirely different mechanism: the fast zigzag diffusion through local patches of parallel aligned mirrors in the lattice. That is, although the average concentration of left and right mirrors are fixed and their left and right orientations occur on the average randomly in the lattice, there will be local fluctuations of the mirror orientations around this average random orientation that tend to align them parallel, either oriented to the left or to the right. In both cases these parallel mirror orientations will speed up the diffusion process, leading to a positive deviation of the diffusion coefficient D from the Boltzmann value D_B.

We estimated the effect of the local concentration fluctuation by computing the diffusion coefficient $\tilde{D}$ corresponding to a lattice with concentration $\tilde{C}$ and then averaging. This assumes that the particle stays long enough in a parallel aligned region that the method of the last section can be used to approximate the local behavior. Defining a fluctuation away from the average concentration $C_L = C_R = C/2$ of the mirror concentrations by $\tilde{\delta}$ through

$$\tilde{C}_L = (C/2)(1+\tilde{\delta}), \quad \tilde{C}_R = (C/2)(1-\tilde{\delta}) \ , \tag{12}$$

where $\tilde{C}_L$ and $\tilde{C}_R$ are the actual concentrations and using the Eqs. (6) and (11), one obtains, for the fluctuating diffusion coefficients $\tilde{D}$, the expression

$$\tilde{D} = \frac{1}{2C(1-\tilde{\delta}^2)} - \tfrac{1}{4} \approx D_B + \frac{\tilde{\delta}^2}{2C} \tag{13}$$

for $\tilde{\delta}^2$ small. Averaging Eq. (13) and assuming that $\langle \tilde{\delta}^2 \rangle = \alpha C$, one finds that $\alpha = \frac{1}{4}$ or

$$D = \langle \tilde{D} \rangle = D_B + \tfrac{1}{8} \ , \tag{14}$$

fits the simulation results very well for $0 < C < 0.8$ (cf. Fig. 3, dashed line). It is interesting to note that around this same concentration the histograms of the closed orbits of the wind particles given in Ref. 8 show a marked change in behavior. On the other hand, the negative de-

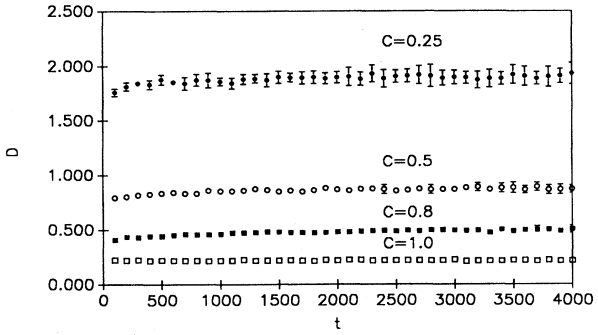

FIG. 2. Time dependence of CD with D defined by Eq. (1), for $C_L = C_R$ and $C = 0.25$, 0.5, 0.8, and 1.0. The error bars in this figure and all the following figures indicate the standard deviations; no error bar means that the deviation is smaller than the size of the symbol.

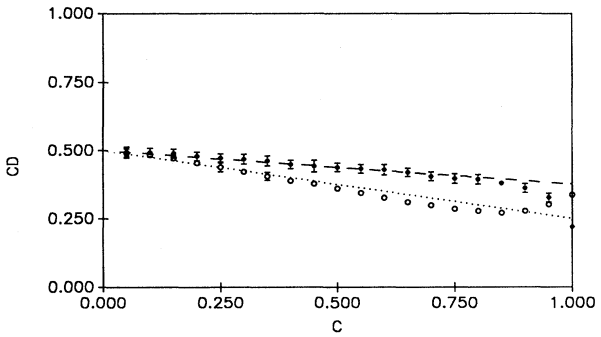

FIG. 3. Concentration dependence of CD at $t = 4000$ (solid circles) for model A and CD' at $t = 2048$ (open circles) for model B for $C_L = C_R$. The dotted (dashed) lines is the Boltzmann result without (with) the fluctuation term added.

viations from D_B found for $C>0.8$ are due to the preponderance of closed orbits at these high concentrations, which slows down the diffusion.

In Fig. 4 a plot is given of the diffusion coefficient D as a function of C_R for $C_L \neq C_R$ and $C=\frac{1}{2}$. The dotted line is given by Eqs. (6) and (10), while the dashed line, given by Eq. (14), agrees well with the data. For $C_L=0$ or $C_R=0$, i.e., when all mirror are parallel, ϕ_B, given by Eq. (10), diverges, so that D is no longer defined. However, as Fig. 4 shows, for very small random mixtures of left and right mirrors a value for D close to D_B is already obtained for all $0<C\leq 1$.

IV. THE DISTRIBUTION FUNCTION AND CLOSED ORBITS

For a normal diffusion process, Fick's law holds, i.e.,

$$\frac{\partial P(\mathbf{r},t)}{\partial t}=D\nabla^2 P(\mathbf{r},t)\ , \tag{15}$$

where $P(\mathbf{r},t)$ is the probability density to find the diffusing particle at $\mathbf{r}$ at time t. The solution of this equation for $P(\mathbf{r},t)$ is a Gaussian distribution function, which implies Eq. (1) for the mean-square displacement. Conversely, however, Eq. (1) does not necessarily imply Eq. (15), i.e., a Gaussian distribution function, as was already pointed out by Gates.[4] In Fig. 5, we plot a typical radial density distribution function for the $C_L=C_R$ case, $\hat{P}(r,t)-2\pi r P(\mathbf{r},t)$, i.e., the probability of finding the particle between r and $r+dr$ at a finite time t. Indeed one clearly sees that the distribution function of the wind particles is not a Gaussian, although $\Delta(t)\sim t$. The non-Gaussian character of $P(\mathbf{r},t)$ is most visible in the peak at the origin and is caused by the large probability for a particle to be trapped in a small finite area near its starting point, i.e., repeating its motion periodically on the lattice in a closed orbit. The "peakedness" of the distribution function can be characterized by the kurtosis[11]

$$K=\frac{\langle \Delta x^4\rangle}{\langle \Delta x^2\rangle^2}-3\ , \tag{16}$$

which vanishes for a Gaussian distribution function. Figure 6 shows the density dependence of K. It is clearly only for very low mirror concentrations, when the diffusion process is Boltzmann-like, that the distribution function approaches a Gaussian. It is interesting to note that, nevertheless, Eq. (1) holds for all concentrations, in spite of the many closed orbits. This is related to another deviation of the distribution function from a Gaussian relevant at large distances. This deviation is due to the fact that the particle diffuses somewhat faster than normal due to the presence of the aforementioned zigzag motion, which appears just to compensate the slower

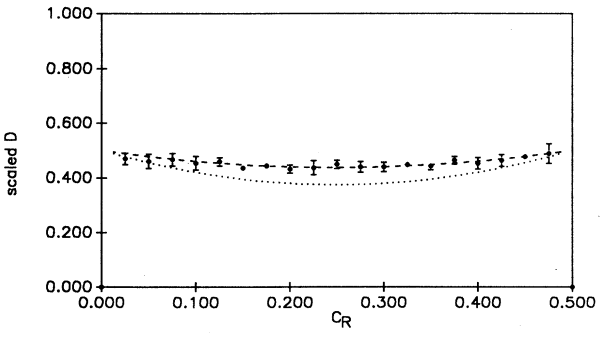

FIG. 4. C_R dependence of the diffusion coefficient D, scaled by $4C_LC_R/C$, for $C_L+C_R=\frac{1}{2}$. The dotted (dashed) line is the Boltzmann result without (with) the fluctuation term added.

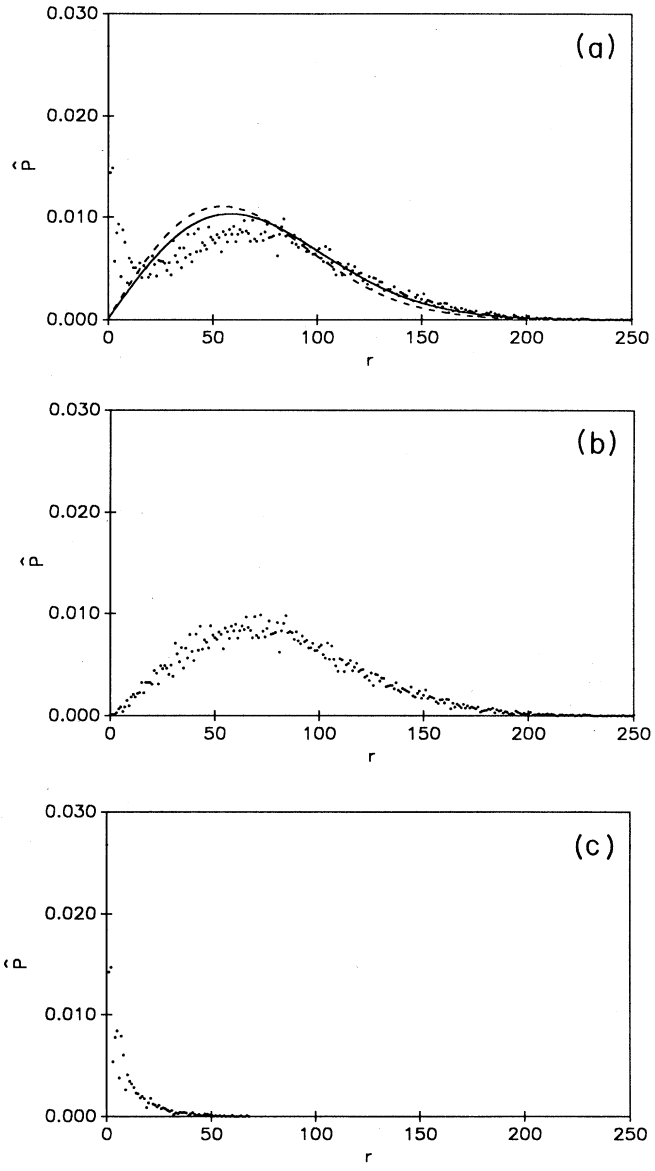

FIG. 5. (a) Typical radial density distribution function $\hat{P}(r,t)=2\pi r P(\mathbf{r},t)$ for $C=0.5$ and $C_R=C_L$ at $t=2000$ (dots). The dashed (solid) line is a Gaussian curve using the Boltzmann (measured) value for the diffusion coefficient; (b) contribution from open orbits; (c) contribution from closed orbits.

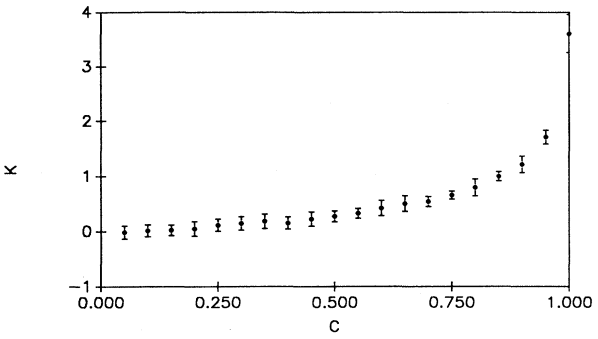

FIG. 6. Concentration dependence of the kurtosis K at $t=4000$.

slower spreading at small distances due to the closed orbits, leading to $\Delta(t)\sim t$, in spite of the non-Gaussian character of the distribution.

V. RELATION WITH THE BOND PERCOLATION PROBLEM

Relations between the wind-tree model and the percolation problem have been noted before.[2–4] For our present model, the precise relation to the bond percolation problem has been pointed out to us by Nienhuis.[12] The mirrors on the original lattice can be considered as the bonds of a bond percolation problem on two sublattices, indicated by dashed and dotted lines, respectively, in Fig. 1. At a given lattice site left and right mirrors belong to a bond of different sublattices. The percolation threshold of these two square sublattices corresponds in our model to a lattice fully occupied by mirrors, so that $C=1$ and $C_L=C_R$, and the bonds of the two sublattices have an equal chance of $\frac{1}{2}$ to be occupied. In this case ($C_L=C_R=\frac{1}{2}$) the trajectory of a wind particle will trace out the boundary of a percolation cluster. In fact, our $C_L=C_R=\frac{1}{2}$ case of a fully mirror occupied lattice is directly related to the ring-forming smart kinetic walk (SKW) without trapping sites of Weinrib and Trugman.[13] In such an SKW, only the origin, i.e., the starting point of the walk, but no other previously visited sites, can be revisited by the walker. Weinrib and Trugman have shown that the ring-forming SKW on a honeycomb lattice traces out the external perimeter of a critical site percolation cluster. They argued that for the mean-square displacement of the N-step walk holds

$$\langle R_N^2\rangle \sim N^{2\nu}=N^{8/7} . \tag{17}$$

This was later proved by Saleur and Duplantier[14] for a square lattice. The difficulty that Weinrib and Trugman noticed with the SKW on a square lattice, viz., that of a self-intersection of the walk at single sites, is eliminated if one considers our mirror model and bond percolation. In that case, a mirror will define the trajectory of a wind particle at a twice visited mirror site unambiguously (cf. Ref. 13, Fig. 4), so that a non-self-intersecting walk results. Coniglio *et al.*[15] have used the interacting self-avoiding random walk to describe the SKW. They showed that the weights of an SKW and a self-avoiding walk (SAW) for a given trajectory are related by

$$W_{\mathrm{SKW}}=W_{\mathrm{SAW}}e^{M\ln 2} , \tag{18}$$

where M is the number of probability 1 steps. In our mirror model, this M is just the number of mirrors visited twice by the wind particle. Assuming then that the tricritical temperature Θ for polymer collapse is equal to the temperature Θ' of Coniglio *et al.*[15–17] and, in addition, that universality holds, the $C=1$ case of our mirror model corresponds to the polymer collapse case of the polymer problem. This is supported by our result that, within the experimental accuracy, we find indeed $\nu=\frac{4}{7}$ for our model.

Furthermore, for our model, Eq. (17) implies asymptotically, that for open orbits

$$\langle \Delta r^2(t)\rangle_o \sim t^{8/7} , \tag{19}$$

where the average is only over open orbits. It has been argued by Nienhuis[12] that the probability $p(t)$, that a particle orbit is still open at a long time t, is given by

$$p(t)\sim t^{-1/7} . \tag{20}$$

We have checked Eqs. (19) and (20) in our model by counting the number of closed and open orbits. Figures 7(a) and 7(b) show that our simulations are consistent with the predictions. Our numerical estimates of the exponent in Eq. (19) is 1.141 ± 0.003 and of the exponent in

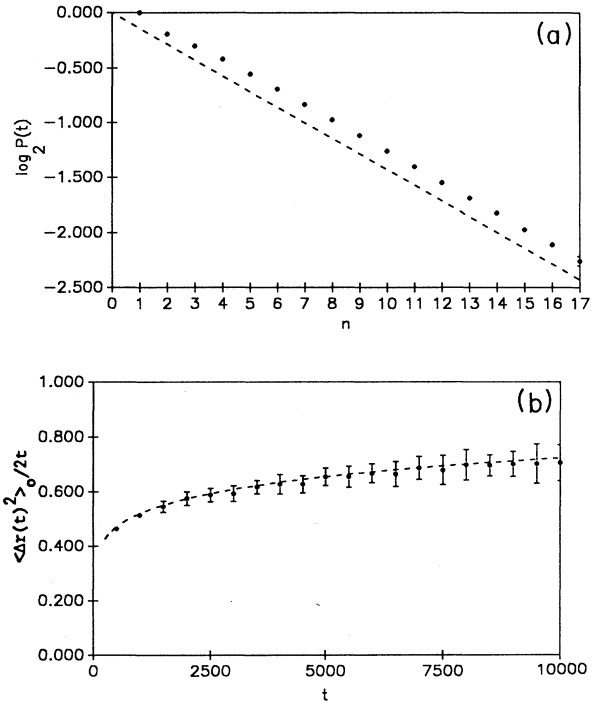

FIG. 7. (a) Logarithmic (base 2) plot of the probability for an orbit still open at time $t=2^n$. The dashed line is a plot of Eq. (17) with proportionality constant equal to 1; (b) plot of $\langle \Delta r(t)^2\rangle_o/2t$, where the dashed line is a function $\sim t^{1/7}$.

Eq. (20) is -0.142 ± 0.003, in agreement with the predicted values.

As pointed out in the Introduction, there are systems for which a critical density, ρ_c, exists, such that for $\rho<\rho_c$, independent particles diffuse (normally or abnormally) through a set of scatterers, but for $\rho>\rho_c$, the particles are always trapped in finite regions of the system. At this critical density then a dynamical phase transition occurs.[10] Such a situation could obtain for the present lattice-gas automaton for $C=1$, since then Eq. (20) implies that every particle orbit eventually (i.e., for $t\to\infty$) closes. Thus, it seems reasonable to conjecture that $C=1$ is the critical density for this lattice gas, since $C_L=C_R=\frac{1}{2}$ coincides with the percolation threshold in the corresponding percolation problem. To check this, we have plotted in Fig. 8 the ratio of the number of closed orbits to those of all (closed and open) orbits as a function of concentration at the fixed time $t=2^{15}$. The curve shown does not quite reach the value 1 at $C=1$, as it is expected to do, since $t=2^{15}$ is not long enough for this to occur. A variation of the present model that appears to exhibit a critical density below $C=1$ is currently under investigation.[18]

VI. THE FLIPPING MIRROR CASE

Finally we will give some results for the flipping mirror model, model B. There are some important differences between this model and model A, the fixed mirror case. First, it is impossible in model B to have the wind particle trapped in a closed orbit, so that one expects a Gaussian distribution function. Second, if we start with more than one wind particle on the lattice, there will be an interaction between these wind particles through the flipping of the mirrors. Thus, for this model, the numerical results will depend on both the wind-particle density and the mirror concentration in the system. In Fig. 9, we plot a typical density distribution function for the flipping mirror model, which is very close to a Gaussian distribution.

In Fig. 3 the density dependence of the diffusion coefficient D' of the flipping mirror model is shown (open circles). D' is obtained by putting randomly about 2600 particles on the 1024×1024 size lattice, using periodic

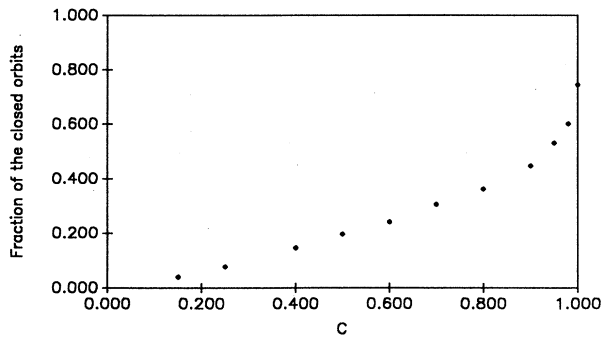

FIG. 8. Ratio of the number of closed orbits at $t=2^{15}$.

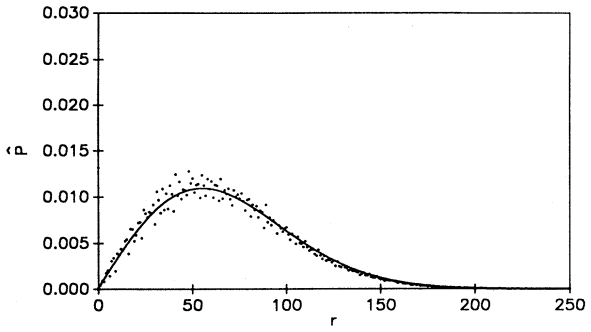

FIG. 9. Radial density distribution function for flipping mirror model for $C=0.5$, $t=2048$ (dots). The solid line is a Gaussian with the measured value of D'.

scatterer boundary conditions. We remark that the deviations of D' from the Boltzmann result D_B are negative for intermediate concentrations and positive for high concentrations. The negative deviations can be related to memory effects connected with such events as ring events, while the positive deviations can be related to the zigzag motions mentioned before. For this we first note that if one extrapolates the values of D' for intermediate concentrations to $C=1$, one arrives at a value of D' close to the value of D for fixed mirrors. Similarly, the actual value of D' at $C=1$ is close to that given for D by Eq. (14), which we shall denote by $\bar{D}$, and which incorporates the effect of zigzag motions. In fact, within the accuracy of our computer simulations, one has for $C=1$,

$$D'=\bar{D}-(D_B-D)=D+(\bar{D}-D_B)\ . \tag{21}$$

This suggests that the increase of the diffusion coefficient D' for the flipping model when the concentration approaches $C=1$ is due to the zigzag motion of the wind particles at these high mirror concentrations, since the difference $(\bar{D}-D_B)$ in Eq. (21) is due to the zigzag motion. One could wonder why this zigzag effect is not present at lower concentrations. The reason is the interaction of the wind particles through close successive collisions with the same mirror. To see this, we distinguish two characteristic lengths: the mean free path l of the wind particles due to their collisions with the mirrors and the average distance a between wind particles. If $a<l$, as is the case at low mirror concentrations, the zigzag effect will disappear, because the positions of the mirrors will be randomized by the successive collisions they suffer with many wind particles. This can be demonstrated experimentally by setting up a close-packed wind-particle region of $50\times50=2500$ wind particles in the center of the lattice. For a short time, $t=500$ say, the wind-particle density in this region will remain high, since the wind particles will not have time to move very far out of this region. As a consequence the diffusion coefficient $D'\approx D_B$, because the mirrors flip very frequently by successive collisions with nearby wind particles. This is confirmed in Fig. 10.

The similarity of the increase of D', due to zigzag motions, and the decrease of D, due to closed orbits, to

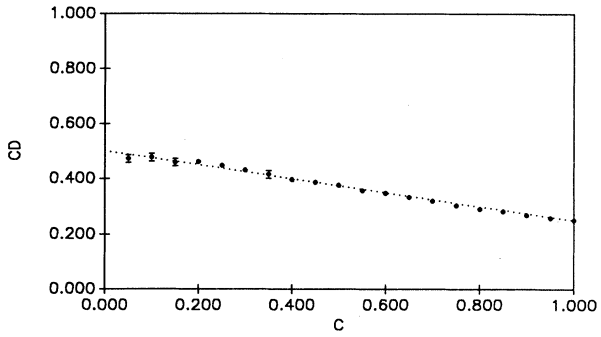

FIG. 10. Concentration dependence of CD' at $t=500$, if the wind particles start in a close-packed region.

their respective values at $C=1$, as seen in Fig. 3, might well be related to the compensation of the contributions of closed orbits and zigzag motion to D, that lead to a mean-square displacement proportional to t in model A, in spite of the non-Gaussian distribution function.

In conclusion, we remark that although we believe that we understand the physical basis of the diffusion processes in the two models discussed in this paper, a quantitative theory beyond Boltzmann, i.e., understanding quantitatively the deviations from the Boltzmann approximation, remains an open question.

ACKNOWLEDGMENTS

The authors are very grateful to Dr. B. Nienhuis for very helpful correspondence concerning the percolation problem. They are also indebted to Professor H. van Beijeren for discussions. This work was performed in part under Department of Energy (DOE) Grant No. DE-FG02-88ER13847.

APPENDIX: DISCRETIZATION EFFECT ON THE TRANSPORT COEFFICIENTS OF LATTICE-GAS FLUIDS

The effect of the space discretization of a lattice on the transport coefficients will be discussed for a two-dimensional lattice with lattice constant b and particles with the same speed v, so that the time τ for a particle to traverse the distance between lattice sites is given by $\tau=b/v$. As in the continuous case, we can associate a dynamical variable $G(t)$ with any transport coefficient L,[19] so that if

$$G(t)=\sum_{n=0}^{N-1} J(n)\tau \,, \tag{A1}$$

where $J(n)$ is the current related to G, then

$$L=\lim_{t\to\infty}\frac{\langle G(t)^2\rangle}{2t} \,, \tag{A2}$$

where $t=N\tau$, and $\langle\ \rangle$ denotes an equilibrium ensemble average. From (A1) follows immediately

$$\langle G(t)^2\rangle=\sum_{n_1=1}^{N-1}\sum_{n_2=0}^{N-1}\langle J(n_1)J(n_2)\rangle\tau^2 \,. \tag{A3}$$

Using stationarity in time, i.e.,

$$\langle J(n_1)J(n_2)\rangle=R(n_1-n_2)=R(n_2-n_1) \,, \tag{A4}$$

one has, with n_1 and $n=n_2-n_1$, as new variables,

$$\begin{aligned}\langle G(t)^2\rangle&=\sum_{n_1=0}^{N-1}\sum_{n_2=0}^{N-1}R(n)\tau^2\\&=2\sum_{n=1}^{N-1}\sum_{n_1=0}^{N-1-n}R(n)\tau^2+tR(0)\tau\\&=2\sum_{n=1}^{N-1}(t-n\tau)R(n)\tau+tR(0)\tau \,.\end{aligned} \tag{A5}$$

In the continuous case the last term would not contribute to $\langle G(t)^2\rangle$, but in the discrete case, considered here, it does. For sufficiently fast decay of $R(n)$,

$$\lim_{t\to\infty}\frac{1}{t}\sum_{n=1}^{\infty}nR(n)\tau^2=0 \,,$$

so that

$$\begin{aligned}L=\lim_{t\to 0}\frac{\langle G^2(t)\rangle}{2t}&=\sum_{\tau=1}^{\infty}R(n)\tau+\tfrac{1}{2}R(0)\tau\\&=\sum_{n=0}^{\infty}\langle J(0)J(n)\rangle\tau-\tfrac{1}{2}\langle J(0)J(0)\rangle\tau \,.\end{aligned} \tag{A6}$$

In (A6), the first term corresponds to the usual Green-Kubo formula for the transport coefficient L, while the second term is a correction due to the discreteness of the lattice. Taking $J=v_x$, (A6) leads directly to Eq. (6) for $\tau=1$.

[1]P. Ehrenfest, *Collected Scientific Papers* (North-Holland, Amsterdam, 1959), p. 229.
[2]E. H. Hauge and E. G. D. Cohen, J. Math. Phys. **10**, 397 (1969).
[3]E. H. Hauge, in *Transport Phenomena,* edited by G. Kirczenow and J. Marro (Springer-Verlag, Berlin, 1974), p. 337.
[4]D. J. Gates, J. Math. Phys. **13**, 1005 (1972); **13**, 1315 (1972).
[5]U. Frisch, B. Hasslacher, and Y. Pomeau, Phys. Rev. Lett. **56**, 1505 (1986).
[6]P. M. Binder, Complex Systems **1**, 559 (1987).
[7]M. H. Ernst and P. M. Binder, J. Stat. Phys. **51**, 981 (1988).
[8]Th. W. Ruijgrok and E. G. D. Cohen, Phys. Lett. A **133**, 415 (1988).
[9]U. Frisch, D. d'Humières, B. Hasslacher, P. Lallemand, Y. Pomeau, and J. P. Rivet, Complex Systems **1**, 649 (1987).
[10]E. G. D. Cohen, in *Théories cinétiques classiques et relativistes, Proceedings of the Colloques Internationaux du Centre National de la Recherche Scientifique,* 1974, edited by M. G. Pichon (Centre Nationale de la Recherche Scientifique, Paris, 1975), p. 269.
[11]See, for example, A. M. Mood, F. A. Graybill, and D. C. Boes, *Introduction to the Theory of Statistics* (McGraw-Hill, New

York, 1974), p. 76.
[12]B. Nienhuis (private communication).
[13]A. Weinrib and S. A. Trugman, Phys. Rev. B **31**, 2993 (1985).
[14]H. Saleur and B. Duplantier, Phys. Rev. Lett. **58**, 2325 (1987).
[15]A. Coniglio, N. Jan, I. Majid, and H.E. Stanley, Phys. Rev. B **35**, 3617 (1987).
[16]P. H. Poole, A. Coniglio, N. Jan, and H. E. Stanley, Phys. Rev. Lett. **60**, 1203 (1988).
[17]B. Duplantier and H. Saleur, Phys. Rev. Lett. **60**, 1204 (1988).
[18]X. P. Kong and E. G. D. Cohen (unpublished).
[19]E. Helfand, Phys. Rev. **119**, 1 (1960).